JOURNAL OF PROPULSION AND POWER
Vol. 11, No. 2, March–April 1995

Penetration and Mixing of Radial Jets in Neck-Down Cylindrical Crossflow

G. Zhu* and M.-C. Lai†
Wayne State University, Detroit, Michigan 48202
and
T. Lee‡
Johns Hopkins University, Baltimore, Maryland 21218

A parametric study of the penetration and mixing of radial jets in a neck-down cylindrical crossflow, which is characteristic of the quick-mix section in a generic tubular rich-burn/quick-mix/lean-burn combustor, is performed numerically. The parameters considered are the jet-to-crossflow momentum-flux ratio, number of injection orifices, neck-down ratio, swirling flow, and aspect ratio and orientation of radial slots. The analysis considers only nonreacting flows in order to concentrate on the fluid mechanics aspect of the processes, using temperature as a passive scalar to characterize the mixing performance. Laser-induced fluorescence experiments were also performed to verify the computational model. The results show that 1) the momentum-flux ratio has the most prominent effects on mixing performance, 2) there is a tradeoff between mixing effectiveness and pressure penalty, 3) the optimal configuration changes with the number of orifices and the slot aspect ratio, 4) an empirical optimal mixing correlation was developed for slotted orifices, 5) swirling flow does not improve mixing or pressure loss, and 6) necked-down sections do not necessarily enhance mixing but produce structural blockage, raising the pressure penalty. The implications of the parametric study on designing optimal mixer geometry are also discussed in terms of temperature and pressure penalty.

Nomenclature

C = experimentally derived constant for single-side injection, 2.5
D = axial flow inlet diameter
D_h = hydraulic diameter
D_{lean} = exit diameter of lean-burn section
J = momentum-flux ratio of the radial jets to the crossflow, $(\rho_j V_j^2)/(\rho_c V_c^2)$
k = turbulent kinetic energy
m = mass flux
N = optimum number of orifice
n = number of radial injection orifice
P_d = dimensional pressure drop across the combustor
P_s = stagnation pressure
r = radial direction
SAR = jet slot aspect ratio, long dimension/short dimension
T = temperature
T_{avg} = average temperature
V = mean velocity in the x (or r) direction for crossflow (or jet flow)
x = axial direction with origin at the center of the injection slot
ΔP = dimensionless pressure drop across the combustor, P_d/P_s
ε = dissipation rate of turbulent kinetic energy
ρ = density of the fluid
σ_T = mass-averaged standard deviation of temperature

Subscripts
c = core flow
i = grid number
j = jets

Received Dec. 4, 1992; revision received June 22, 1994; accepted for publication July 15, 1994.

*Research Assistant, Department of Mechanical Engineering. Student Member AIAA.
†Associate Professor, Department of Mechanical Engineering. Member AIAA.
‡Associate Research Scientist, Department of Chemical Engineering.

Introduction

RAPID mixing of two streams of fluid is frequently required in energy systems and in chemical or manufacturing processes. One particular type of rapid mixer that has a simple geometry and does not require mechanical mixing or swirling is the radial mixer, in which radial jets are injected from orifices into cylindrical crossflow. The cylindrical cross section is usually reduced at the jet injection location in order to provide a low-pressure core to enhance penetration of the radial jets.

One particular application of the radial mixer is the low-emission axially staged combustor,[1] or the rich-burn/quick-mix/lean-burn (RQL) combustor.[2] In this type of combustor, combustion is initiated in a fuel-rich zone at equivalence ratios between 1.2–1.8, thereby reducing NO_x formation by lowering the combustion temperature and depleting the available oxygen. Bypass combustion air is introduced in a quick-mix section, and lean combustion occurs downstream at an overall equivalence ratio between 0.5–0.7. The quick-mix section of a tubular RQL combustor is essentially a radial mixer. The neck-down area, in addition to enhancing mixing and preventing backflow, serves to reduce residence time at the mixer. However, care must be taken to achieve quick, uniform, and complete mixing of the hot rich-zone products to avoid the formation of high-temperature and subsequent thermal NO_x, which takes place at the stoichiometric conditions,[3] and local hot spots that deteriorate the overall emission and the material performance. Previous investigations of rich/lean combustors for heavy fuel applications[2-4] have clearly shown the sensitivity of overall emission to the quick-mix section. It is the performance of the quick-mix step, and achieving it at the cost of minimum pressure loss, which holds the key to a successful RQL combustion process.

Although previous studies of gas turbine dilution-hole aerodynamics[5-11] contribute to our understanding of the jet-in-crossflow process in general, the radial mixer has some unique characteristics that are still not well understood. For example, the time and space allocated are so short, and the bulk flow rate of the mixing jets is so large, that the momentum-flux ratio of the jet to the crossflow must be in the range of 15–60. Therefore, similar to gas turbine dilution hole aerodynamics, the momentum-flux ratio is expected to be the most prominent control parameter for mixing performance. However, the optimal momentum-flux ratio for any given geometry remains unclear. Different dilution orifice designs (single or multiple lines of circular holes, axial, inclined, or staggered slots) have also appeared in the literature.[2,12-16] However, the effects of geometric parameters such as the number of injection orifices, slot aspect ratios, and slot orientation on the mixing performance remain unclarified. Also, the issues of pressure penalty and neck-down ratio, and the swirling flow in the axial crossflow need to be examined.

The objective of this article is to study numerically the effects of radial jets on the penetration and mixing performance of a generic symmetric RQL quick-mix section. Typical high-pressure, high-temperature airflow properties for a combustor, similar to those proposed by Talpallikar et al.,[12] are used to characterize the jets and crossflow in the present study. However, in order to concentrate on the fluid mechanics aspect of the flow process, only nonreacting flows were considered in the present study. Furthermore, since the mass-flux ratio was kept constant, the average temperature thereby serves as a passive scalar for the mixing process for adiabatic wall boundary conditions. Two types of jet slots were considered: 1) rectangular straight slot aligned in the streamwise direction and 2) slanted slot that is formed by twisting the straight slot with a certain angle. The parameters considered are the jet-to-mainstream momentum-flux ratios J, the number of injection orifices n, and the aspect ratios of the slotted orifices, SAR. The equivalence ratio was kept constant. The effects of necked-down ratio, swirling crossflow, and slanted slot on the penetration and mixing performance are examined for selected cases. The implications of the parametric study on designing optimal mixer geometry are also discussed in terms of temperature uniformity and pressure penalty. Also, pulsed laser-induced fluorescence experiments were also performed to verify the computational results at selected parametric conditions.

Numerical Approach

A steady-state three-dimensional Navier-Stokes solver[12] was used to investigate radial mixer performance by simulating the nonreacting flowfield in a generic tubular RQL combustor quick-mix section. The computation is based on the finite volume formulation and a variant of the pressure-based SIMPLEC[17] algorithm. The governing equations are formulated using a fully implicit and strongly conservative formulation, and solved with a modified form of Stone's strongly implicit solver.[18] An upwind differencing scheme was used for the convection terms. Turbulence properties are modeled using the k-ε model[19] with wall functions. Typically, the residuals drop four to five orders of magnitude within two hundred iterations, without tuning of the under-relaxation coefficients. Slanted slots and swirling flow cases, however, have slower convergence speed. These usually require more than one or two thousand iterations.

The base geometry consists of three components: 1) the crossflow inlet, 2) the neck-down injection section, and 3) an enlarged mixing section, with a 6- by 5- by 7-in- (0.152- by 0.127- by 0.178-m-) diam variations. The lengths of the straight cylindrical sections were 0.076, 0.228, and 0.127 m, respectively; the lengths of the converging and diverging cylindrical sections were 0.22 and 0.066 m, respectively. The mixing performance was characterized using the mass-weighted-standard-deviation of temperature distribution σ_T at one-half of the inlet diameter downstream of the quench-air injection location. The σ_T is defined as follows:

$$\sigma_T = \left[\frac{\sqrt{\sum_i m_i (T_i - T_{\text{avg}})^2}}{\sum_i m_i} \Big/ T_{\text{avg}} \right] \tag{1}$$

where T_i and m_i are the temperature and mass flux in each computational grid cell i, respectively. Optimal mixing should result in the most uniform temperature distribution, or minimum σ_T. In addition to temperature uniformity, pressure loss was also an important consideration for combustor performance, therefore, it is also taken into account by keeping track of the stagnation pressure difference ΔP across the computation domain. Equation (1) could also be normalized using $T_{\text{avg}}(1 - T_{\text{avg}})$ instead of T_{avg} as proposed by Dimotakis and Miller,[20] in order to bound σ_T between 0 and 1, allowing comparisons of cases where mass-flux ratio is not fixed.

The parameters considered in the present study are the jet-to-mainstream momentum-flux ratios (J = 2–64), the number of injection orifices (n = 2–12), and the aspect ratios of the mixing jet slots (SAR = 1 to 4). The mixing sections are interchangeable, each has a different geometry. The overall mass-flow ratio of jet-to-crossflow (equivalence ratio) is kept constant. The effects of neck-down ratios, swirling crossflow, slanted slot, and turbulent intensity of the jet on the mixing performance were also studied for selected cases.

Grid System

A cylindrical body-fitted system was used for the numerical study. Due to the symmetry of the radial jets in crossflow, the computation domain covers only half of the pie-section, which is sandwiched between a periodic boundary condition plane (between the jets) and a symmetry plane (at the jet center). For cases with slanted slots or swirling crossflow, however, a whole pie section (sandwiched between two periodic boundaries) was used for the computation domain. A transfinite interpolation procedure was used to generate the grids for the slanted-slot case. Typical grid systems used in the straight-slot and slanted-slot cases are shown in Fig. 1. Grid density converges to the jet center and to the wall to resolve the strong velocity gradients in these areas.

The grid system must be changed with respect to the number of injection orifices, since the physical dimensions of the pie-section change with the number of orifices in reverse order. The grid system must also be modified to correspond to the change in slot aspect ratio. Furthermore, since the overall mass-flow ratio of jet to crossflow (equivalence ratio) is kept constant, the orifice dimension will also change with the momentum-flux ratio. As a result, the grid system must be changed for every parameter considered. Grid-sensitivity was studied using the test case with J = 24, n = 6, and SAR = 1. Visual inspection of the flow pattern showed very little change when the grid density reached 10,000 for the computation domain. Typical sensitivity of σ_T to the grid density is shown in Fig. 2. This figure shows that less than 2% of variation in σ_T was found when the grid density is between 10,000–100,000 for the computation domain. Most of the grid densities of the test matrix are in this range; for the present parametric study the current grid system is felt to be sufficient.

Boundary Conditions

For simplicity, a uniform velocity profile is prescribed at both inlets of the jet and the mainstream. The sensitivity of the solution to the inflow turbulence properties was also studied by prescribing different turbulence intensities at the jets.[21] The results show that the initial turbulence intensities have some influence on the overall flowfield. This is plausible, since

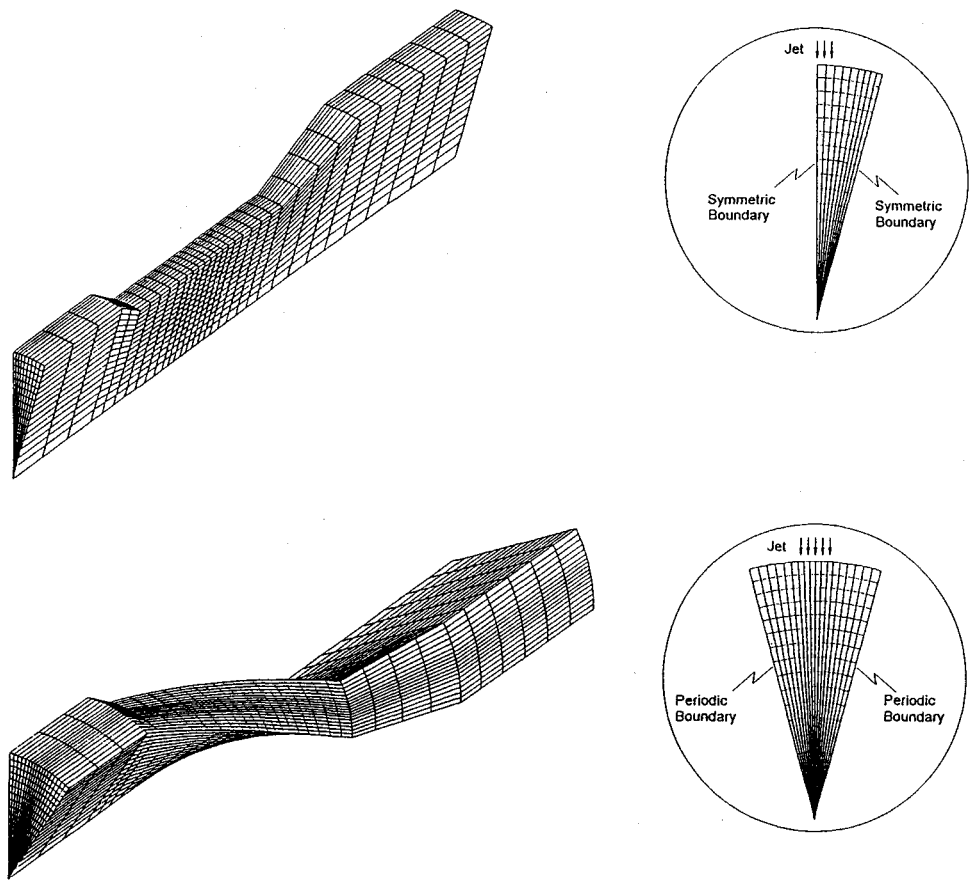

Fig. 1 Typical grid system: a) straight and b) slanted slots.

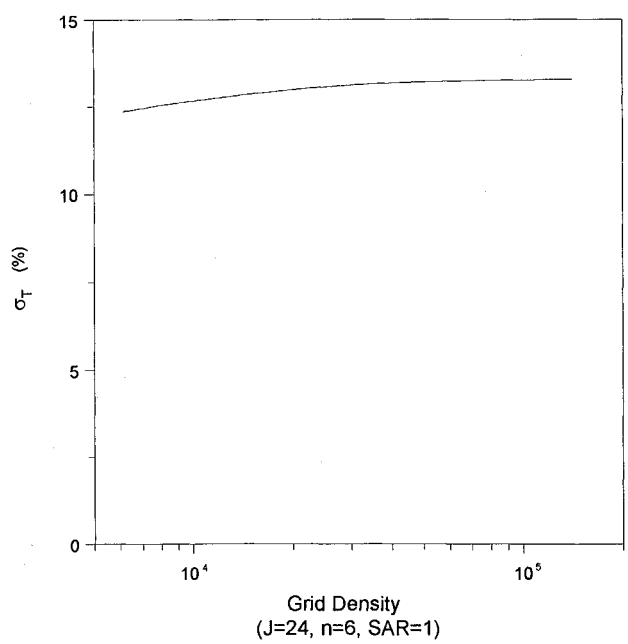

Fig. 2 Typical grid sensitivity on the results of σ_T for $J = 24$, $n = 6$, and SAR = 1.

the turbulence structure of the jets will influence the momentum and mass transport processes. Also, in order to find the appropriate boundary conditions, a computation domain incorporating an outer annular plenum chamber that supplies the mixing jets and an inner cylindrical core was used. The two regions were separated by the cylindrical liner, and communicate only through the slot. Cell blockage technique and wall function were invoked to simulate the presence of the cylindrical liner. The convergence history was very slow.

Table 1 Inlet boundary conditions

	Crossflow	Jet
Velocity, m/s	35.4	Varied
Density, kg/m^3	5.82	1.864
Temperature, K	2221	811
Turbulence intensity, $\%D_h$	4	16.2

However, when convergence occurs, the averaged turbulent intensities and dissipation values at the jets inlet were then used as the boundary conditions for the parametric study. The inlet boundary conditions are summarized in Table 1.

Experimental Approach

Pulsed planar laser-induced fluorescence (PLIF) flow-visualization experiments were carried out to validate the computational results. A scaled-down test model, made of Pyrex® glass, with a 3- by 2.5- by 3.5-in. dimension was used in the present experiment. The model was positioned vertically. The necked-down mixing section is interchangeable, each with a different geometry. Figure 3 shows the schematic of the experimental setup. The water flow were gravity-fed to maintain at a steady and constant flow rate throughout the experiment. The mixing jets were fed through an annular plenum around the cylindrical sections. Baffles and flow straighteners were installed inside the plenum to ensure uniform distribution of jet flows around the quick-mix section. The overall mass-flux ratio of jet-to-crossflow (equivalence ratio) is kept constant (1.92). Also, limited by the flow capacity, Reynolds numbers of both the cylindrical crossflow and the mixing were in the range of 5×10^3 to 1.0×10^4.

Kodak dye Styryl-7 was added to the axial flow supply tank and was well-stirred before commencing test. The dye molecules fluoresce when they are illuminated by a Nd-YAG pulsed laser light-sheet passing through the selected test sec-

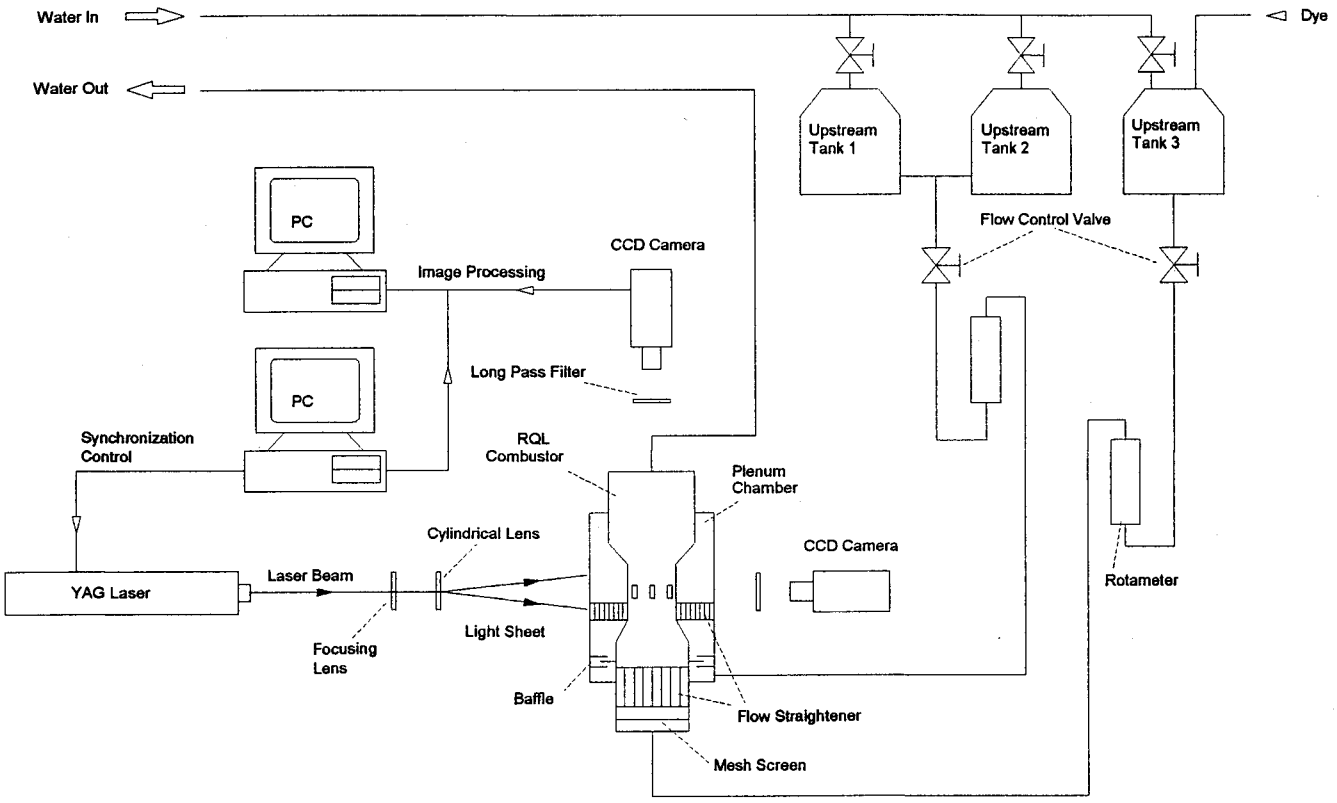

Fig. 3 Schematic of the pulsed PLIF experimental setup.

tion. Second harmonic of the YAG laser at a wavelength of 532 nm was used to excite the dye whose absorption spectrum peaks at 704 nm. The pulse duration was set at 10 ns. Long-pass filter with a cutoff wavelength at 630 nm was used to reduce the background noise due to scattering. The image in the axial or radial cross sections, which indicate the instantaneous mixing processes, were digitized using a Sierra Scientific CCD camera that was synchronized with the laser pulse through a specially designed computer-controlled time-delay system.

Results and Discussions

Computational Results

Effects of Momentum-Flux Ratio

Figure 4 shows the results of σ_T as a function of momentum-flux ratio for a six-slot geometry ($n = 6$), with a slot aspect ratio of 4. The corresponding predicted velocity vector plots and the isotherm contours (at 100 K interval) at the symmetry plane are shown in Figs. 5 and 6, respectively. Figures 5 and 6 show that at low J, penetration is limited and colder fluid is confined to the wall region, and that the degree of penetration increases with J. However, as a critical momentum-flux ratio is exceeded, a recirculation region starts to form in the upstream of the impinging jets that results in overpenetration and undesirable upstream mixing, and consequent blockage effects. In this case, the radial temperature distributions at the downstream section is now reversed (for the overpenetration case), i.e., the colder fluid is in the center region. Figure 4 shows two minimum points of σ_T: one point at $J = 10$, and the other is at $J > 64$ (not shown in this figure). For $J > 10$, overpenetration occurs and is indicated by dashed line.

From the analysis of gas turbine dilution aerodynamics, Holdeman et al.[7,8,22–26] have shown that temperature distributions are similar when J and orifice spacing are coupled, and that optimal mixing in a can ensues the following expression:

$$n = (\pi\sqrt{2J}/C) \tag{2}$$

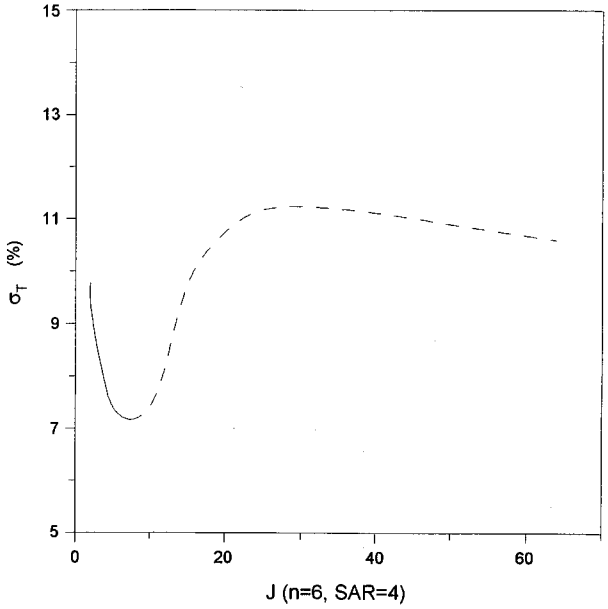

Fig. 4 Effect of J on σ_T for $n = 6$ and SAR = 4. Dashed line indicates overpenetration.

and the optimal momentum-flux ratio is

$$J = (C_n/\pi)^2/2 \tag{3}$$

where $C = 2.5$ is an experimentally determined constant. When Eq. (3) was plotted in Fig. 10, good agreement with the square-orifice case prevailed, in spite of the neck and expansion of the cross section. For slotted orifices, however, Eq. (3) needs to be modified by scaling down the constant C with respect to slot aspect ratio.

Effects of Number of Injection Orifices and Slot Aspect Ratios

Figure 7 shows the effect of momentum-flux ratio on σ_T at different straight-slot aspect ratios and number of orifices.

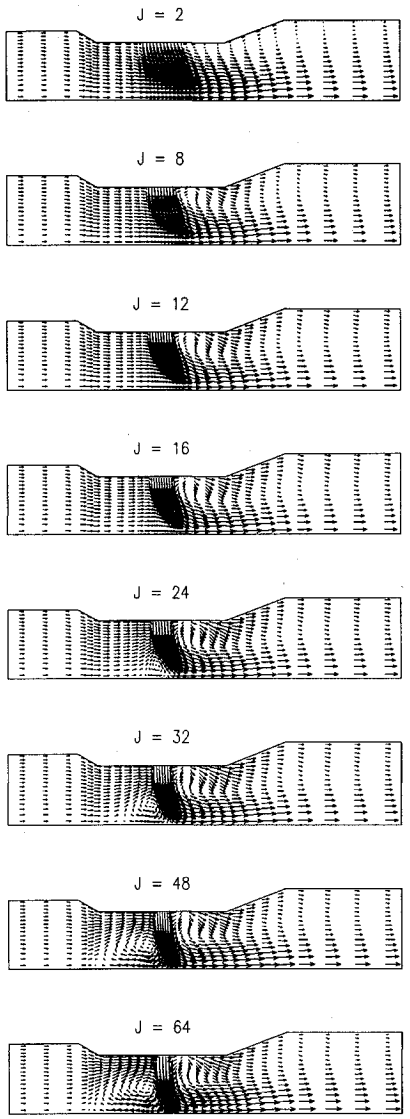

Fig. 5 Velocity vector as a function of J at symmetry plane for n = 6 and SAR = 4.

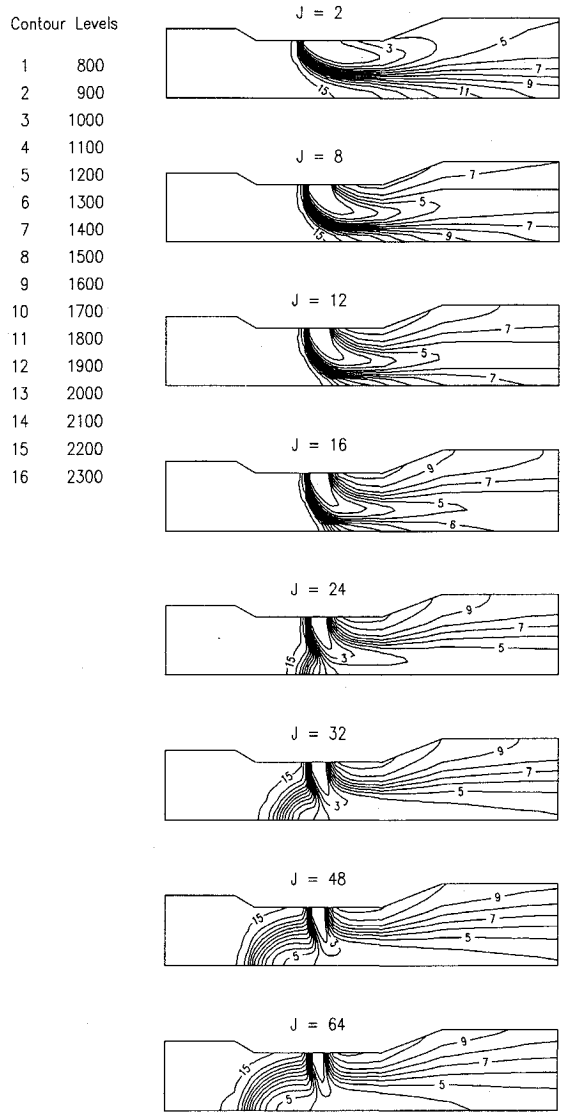

Fig. 6 Isotherm contour as a function of J (at 100 K interval) at symmetry plane for n = 6 and SAR = 4.

The results show that the optimal configuration changes with the slot aspect ratios and with the number of injection orifices. The σ_T curves show a similar trend in these figures; some cases show that the lowest σ_T values are obtained in the overpenetration region (dashed line) at large J. The overpenetration is always accompanied by upstream mixing and high pressure losses, which is not desirable for combustor applications.

Figure 8 shows the stagnation pressure drop across the combustor chamber as a function of momentum-flux ratio at different straight-slot aspect ratios and numbers of orifices. The results show that pressure drop is primarily a function of momentum-flux ratio and increases almost linearly with J. The pressure drop seems to decrease slightly with increasing orifice number. In other words, ΔP is weakly dependent on n, especially when the aspect ratio is close to one.

Optimal Design

While the momentum-flux ratio has the most substantial effects on mixing performance, the optimal momentum-flux ratio required to achieve maximum mixing performance was found to be a strong function of a given configuration (see Fig. 7). Figure 9 shows the minimum σ_T and the associated minimum ΔP plotted against the number of holes at different slot aspect ratios. The corresponding minimum momentum-flux ratios required to achieve minimum σ_T at different SAR values are shown in Fig. 10. Figure 10 shows that there is a good agreement between the present calculation for SAR = 1 (indicated by open triangles) and by that using Eq. (3) (dashed line). An optimal momentum-flux ratio for slotted orifices (i.e., indicated by square, triangle, and rhombus symbols in Fig. 10) can be derived as follows:

$$J = 0.3n^2/\mathrm{SAR}^a \tag{4}$$

where a = 0.4–0.5. Figures 9 and 10 demonstrate a tradeoff between mixing performance and pressure penalty. It shows that although σ_T can be as low as 5.5 (see Fig. 9a), the overall optimal condition may only be 6.5, as in the case of SAR = 4, n = 8, and J = 12.

Effects of Slanted Slots and Swirl Number

Slanted slots are expected to generate swirl and enhance mixing. The primary zone of a conventional combustor usually utilizes swirler for fuel/air mixing. It is interesting to know the effects due to these swirling flows. Therefore, a 30-deg slanted-slot case and a straight-slot case with a solid body rotation prescribed at the inlet (swirl number = 1, excluding the pressure thrust term) are compared with the nonswirling case; all cases have the same number of orifices (n = 12) and aspect ratio (SAR = 4). Because the performance of the

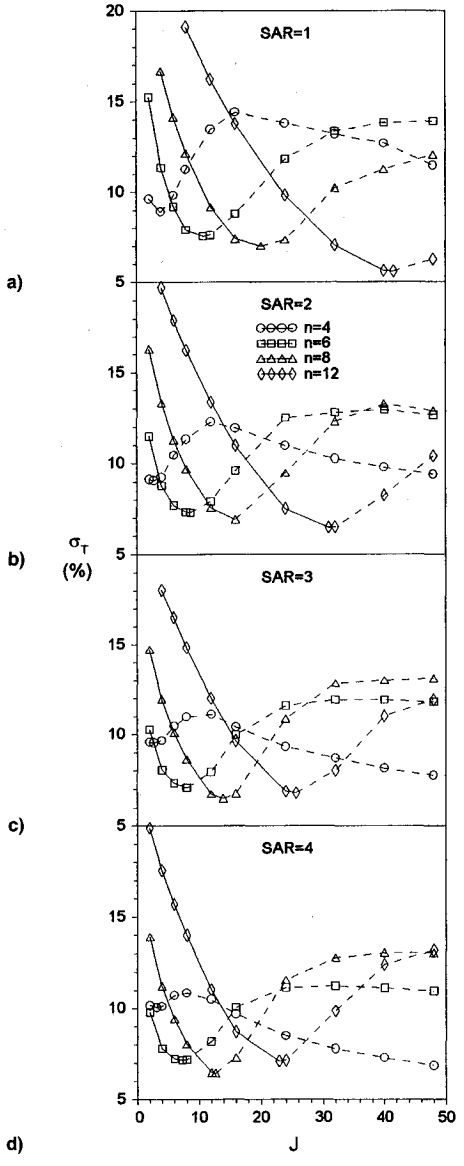

Fig. 7 Effect of J on σ_T at different n values. SAR = a) 1, b) 2, c) 3, and d) 4.

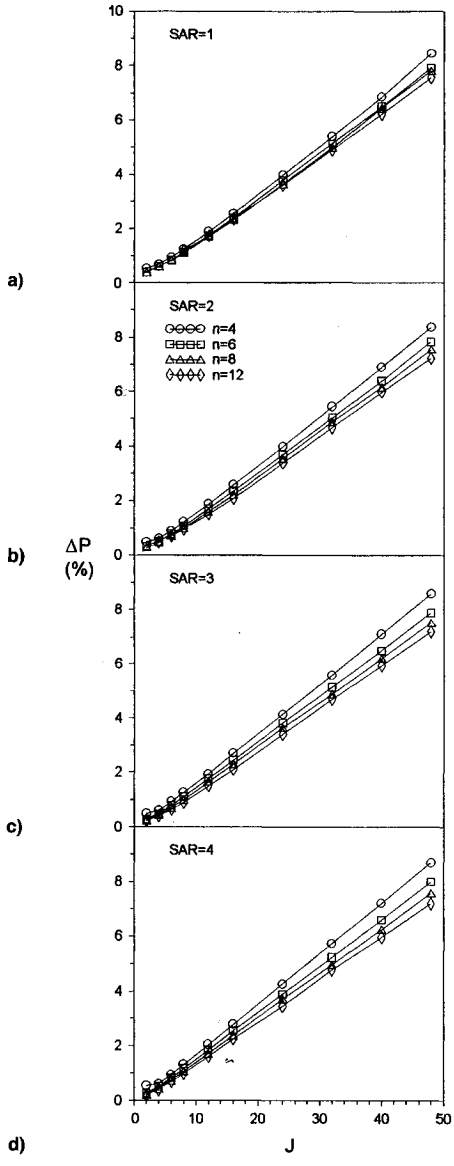

Fig. 8 Effect of J on ΔP at different n values. SAR = a) 1, b) 2, c) 3, and d) 4.

isotropic k-ε model may be limited in strongly swirling flows,[27] the current study should be treated as qualitative.

Figure 11 shows the effects of momentum-flux ratio on σ_T and ΔP for $n = 12$ and SAR = 4 for different slot geometries. All swirling flows (indicated by triangular and square symbols) have significantly higher σ_T for practical momentum-flux ratio ranges and higher pressure loss compared to the mixing performance without swirling flow (indicated by circular symbols). This is probably due to the penetration impedance and diversion that the jets suffered from the swirling flow. Also, concentric counter-rotating flow patterns were observed for the two swirling flow cases shown in Figs. 12 and 13. These figures show that while the slanted-slot cases have a stronger swirling velocity at the outer region (Fig. 12b), the straight-slot cases with swirling crossflow have a stronger swirling velocity in the center region (Fig. 13b).

Effects of Neck-Down Ratio

Figure 14 shows the effects of neck-down ratio on σ_T and ΔP at two different expansion sections for $J = 24$, $n = 8$, and SAR = 4. The results indicate that necked-down section does not necessarily enhance mixing (Fig. 14a), but produces structural blockage, raising the pressure penalty (Fig. 14b). The present results are similar to those reported by Smith et al.[28] Smith et al. found that neck-down sections did not alter the dimensionless mixing significantly, except that it made the region physically smaller and increased the pressure drop. Two different expansion sections are also compared in Fig. 14. One has a larger diffuser angle ($D_{\text{lean}} = 7$) than the other ($D_{\text{lean}} = 6$). The effect of the diffuser angle was not very significant for the cases studied; either the separation flow was not yet dominant or it was suppressed by the axisymmetric constants of the sectional computation domain.[27] Pressure drop across the jet inlets and the exit is also larger than that calculated.

Experimental Results

Figures 15a, 15b, and 15c show the pulsed PLIF images at both axial and radial ($x/D = 0$ and $x/D = 0.5$) sections, respectively, for an overpenetrating case with $J = 32$, $n = 8$, and SAR = 4. Figure 16 shows the results of the underpenetrating case with $J = 6$, $n = 8$, and SAR = 1. The results show that despite the large eddy structures that dominate the mixing process (mainly due to the low-flow Reynolds number used in the present experiment), the general features of over- and underpenetration and jet mixing are clearly visible. In other words, the experimental results again demonstrate that the momentum-flux ratio is the most significant flow variable

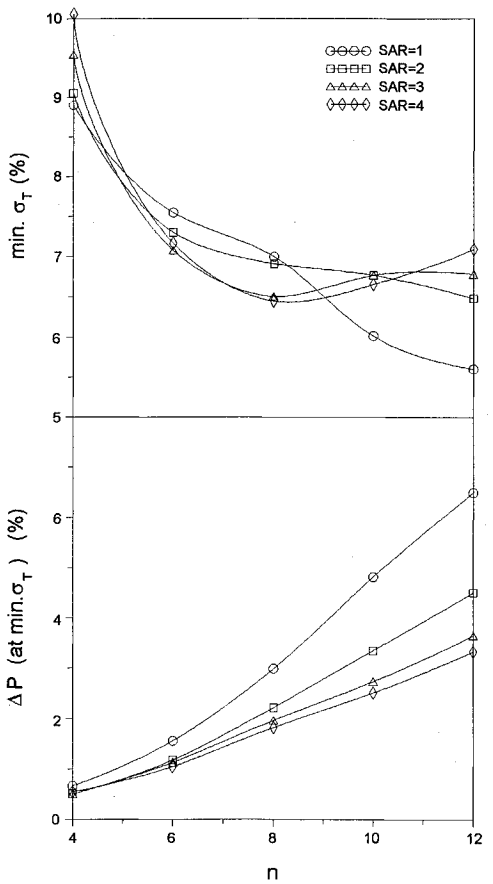

Fig. 9 Effect of n on minimum σ_T and on ΔP required to achieve minimum σ_T at different SAR values.

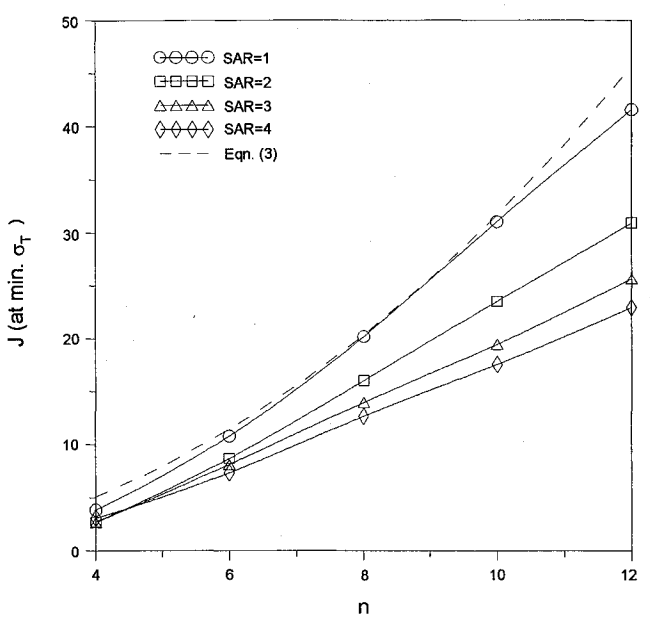

Fig. 10 Effect of n on minimum J required to achieve minimum σ_T at different SAR values.

affecting mixing performance (Figs. 15a, 15b, 16a, and 16b). Information of the instantaneous scalar mixing processes is also given in these pulsed PLIF results. These figures also indicate that there is a good agreement between the general flow characteristics depicted by the instantaneous PLIF images (Figs. 15b and 16b) and the time-averaged computational results (Figs. 5f and 5b), despite the low Reynolds number used in the present experiment. However, long-exposure or

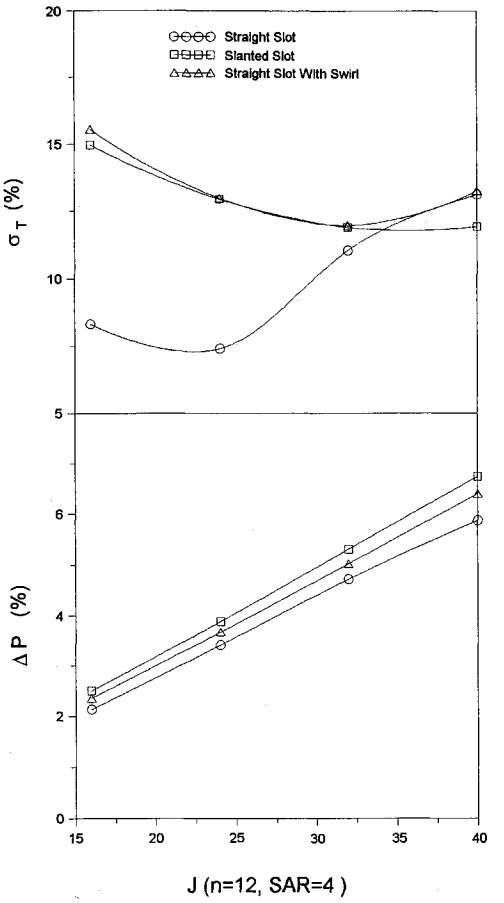

Fig. 11 Effect of J on σ_T and ΔP for n = 12 and SAR = 4.

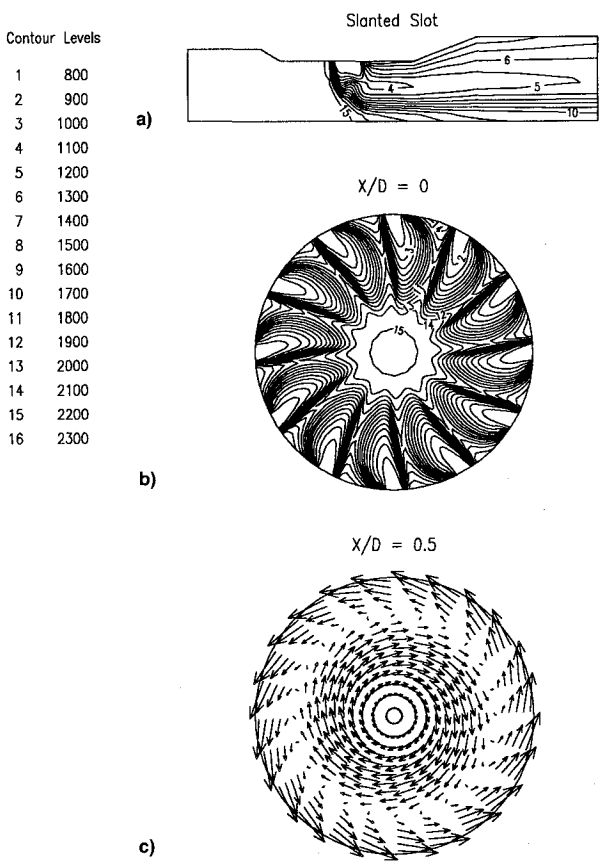

Fig. 12 Flow characteristics of the slanted-slot cases: a) axial and b) radial isotherm contours at x/D = 0, and c) radial velocity vector plots at x/D = 0.5.

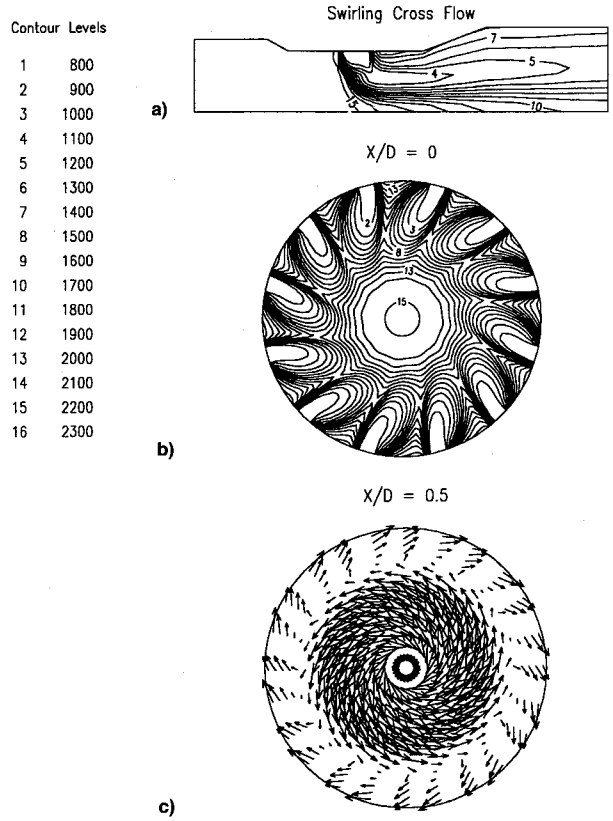

Fig. 13 Flow characteristics of the straight-slot cases with imposed swirling crossflows: a) axial and b) radial isotherm contours at x/D = 0, and c) radial velocity vector plots at x/D = 0.5.

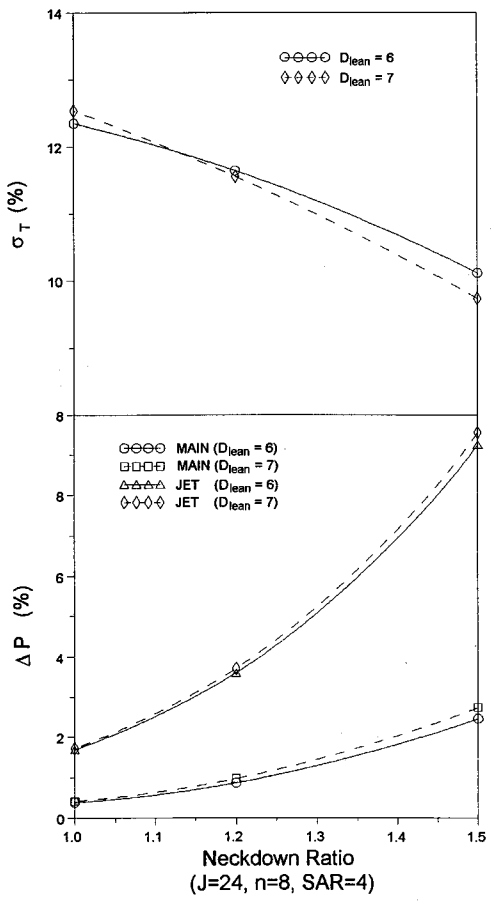

Fig. 14 The effects of neck-down ratio on σ_T and ΔP at different D_{lean} values for J = 24, n = 8, and SAR = 4.

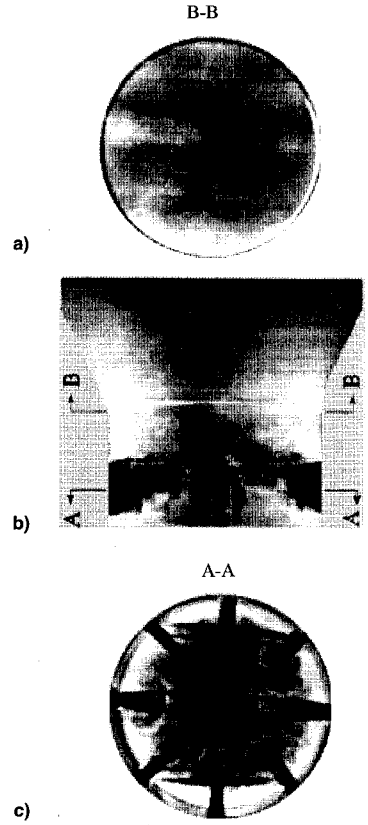

Fig. 15 Images of the flow visualization results for an over-penetrating case with J = 32, n = 8, and SAR = 4: a) radial section at the jet centerline (x/D = 0), b) axial section with flow direction from top to bottom, and c) radial section at half the diameter downstream (x/D = 0.5).

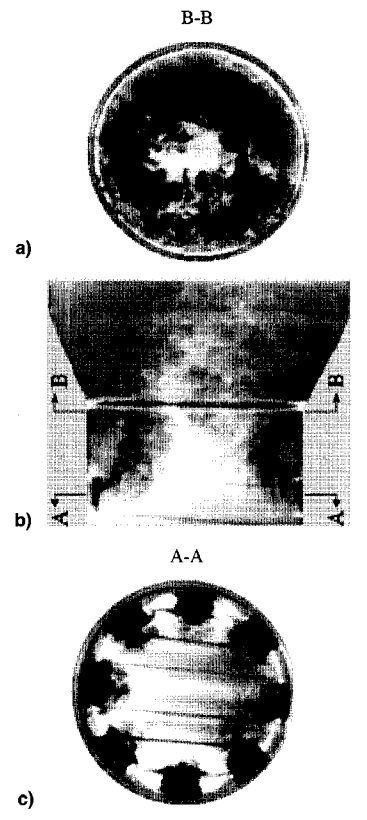

Fig. 16 Images of the flow visualization results for an underpenetrating case with J = 6, H = 8, and SAR = 1: a) radial section at the jet centerline (x/D = 0), b) axial section with flow direction from top to bottom, and c) radial section at half the diameter downstream (x/D = 0.5).

multiple shots are needed to obtain a qualitative comparison between the experimental results and the computational model.

Conclusions

A parametric study of the effects of the jet-to-mainstream momentum-flux ratio, the number of orifice, neck-down ratio, swirling crossflow, and slot aspect ratio on the penetration and mixing of radial jets in necked-down cylindrical crossflow was performed, and we draw the following conclusions:

1) Although the momentum-flux ratio has the most pronounced effects on mixing performance, the optimal jet-to-mainstream momentum-flux ratio J required to achieve maximum mixing performance is different for each configuration.

2) There is a tradeoff between mixing effectiveness and pressure penalty. Also, the pressure drop is primarily a linear function of J.

3) The optimal configuration changes with number of orifices and slot aspect ratio.

4) The correlation for optimal mixing proposed by Holdeman et al.[26] for circular dilution holes was found to be also applicable for square orifices in a tubular RQL geometry, but needs to be modified for rectangular or slanted slots.

5) An empirical optimal mixing correlation was developed for slotted orifices.

6) Swirling flow does not improve mixing or pressure loss.

7) Neck-down section does not necessarily enhance mixing, but produces structural blockage, raising the pressure penalty.

8) There is good agreement between the computational and qualitative experimental results.

Acknowledgments

The authors wish to acknowledge the financial support of Wayne State University and Wayne State Institute of Manufacturing Research.

References

[1]Lefebvre, A. W., "Gas Turbine Combustion," McGraw-Hill, New York, 1983.

[2]Novick, A. S., and Troth, D. L., "Low NO_x Heavy Fuel Combustor Concept Program," NASA CR-165367, 1981.

[3]Shaw, R. J., "Engine Technology Challenges for a 21st Century High Speed Civil Transport," NASA TM 104363, 1991.

[4]Rosfjord, T. J., and Kemp, F. S., "Final Report Low NO_x Heavy Combustor Concept Program Phase 1A Coal Gas Addendum," NASA CR-165577, 1982.

[5]Wittig, S. L. K., Elbahar, D. M. F., and Noll, B. E., "Temperature Profile Development in Turbulent Mixing of Coolant Jets with a Confined Hot Cross-Flow," *Journal of Engineering for Gas Turbines and Power*, Vol. 106, No. 1, 1984, pp. 193–198.

[6]Holdeman, J. D., Walker, R. E., and Kors, D. L., "Mixing of Dilution Jets with a Hot Primary Air Stream for Gas Turbine Combustors," AIAA Paper 73-1249, 1973.

[7]Holdeman, J. D., Srinivasan, R., Coleman, E. B., Meyers, G. D., and White, C. D., "Experiments in Dilution Jet Mixing Effects of Multiple and Non-Circular Orifices," AIAA Paper 85-1104, 1985.

[8]Holdeman, J. D., Srinivasan, R., Reynolds, R., and White, C. D., "Studies of the Effects of Curvature on Dilution Jet Mixing," *Journal of Propulsion and Power*, Vol. 7, No. 2, 1991, pp. 11–19.

[9]Srinivasan, R., Coleman, E., and Johnson, K., "Dilution Jet Mixing Program," NASA CR-174624, 1984.

[10]Srinivasan, R., Coleman, E., and Johnson, K., "Dilution Jet Mixing Program Supplementary Report," NASA CR-175043, 1986.

[11]Carrotte, J. F., and Stevens, S. J., "The Influence of Dilution Hole Geometry on Jet Mixing," *Journal of Engineering for Gas Turbines and Power*, Vol. 112, No. 1, 1990, pp. 73–79.

[12]Talpallikar, M. V., Smith, C. E., and Lai, M.-C., "Rapid Mixing Concepts for Low Emission Combustors in Gas Turbine Engines," NASA CR NAS3-25834, 1990.

[13]Ferrell, G. B., and Lilley, D. G., "Deflected Jet Experiments in a Turbulent Combustor Flowfield," NASA CR-1174863, 1985.

[14]Hatch, M. S., Sowa, W. A., Samuelsen, G. S., and Holdeman, J. D., "Jet Mixing into a Heated Cross Flow in a Cylindrical Duct: Influence of Geometry and Flow Variations," AIAA Paper 92-0773, 1992.

[15]Oechsle, V. L., Mongia, H. C., and Holdeman, J. D., "A Parametric Numerical Study of Mixing in a Cylindrical Duct," AIAA Paper 92-3088, 1992.

[16]Kroll, J. T., Sowa, W. A., Samuelsen, G. S., and Holdeman, J. D., "Optimization of Circular Jets Mixing into a Heated Crossflow in a Cylindrical Duct," AIAA Paper 93-0249, 1993.

[17]Van Doormall, J. P., and Raithby, G. D., "Enhancement of the SIMPLE Method for Predicting Incompressible Fluid Flows," *Numerical Heat Transfer*, Vol. 7, No. 2, 1984, pp. 147–163.

[18]Stone, H. L., "Iterative Solution of Implicit Approximations of Multi-Dimensional Partial Differential Equations," *Journal of Numerical Analysis*, Vol. 5, No. 3, 1968, pp. 530–558.

[19]Launder, B. E., and Spalding, D. B., "The Numerical Computation of Turbulent Flows," *Computational Mathematics in Applied Mechanics and Engineering*, Vol. 3, No. 1, 1974, pp. 269–289.

[20]Dimotakis, P. E., and Miller, P. L., "Some Consequences of the Boundedness of Scalar Fluctuations," *Physics of Fluids A*, Vol. 2, No. 11, 1990, pp. 1919, 1920.

[21]Zhu, G., "Numerical and Experimental Study of Flowfields in Ultra Flow Emission Combustors," Ph.D. Dissertation, Mechanical Engineering Dept., Wayne State Univ., Detroit, MI, 1993.

[22]Holdeman, J. D., Srinivasan, R., and Berenfeld, A., "Experiments in Dilution Jet Mixing," *AIAA Journal*, Vol. 22, No. 10, 1984, pp. 1436–1443.

[23]Holdeman, J. D., and Srinivasan, R., "Modeling Dilution Jet Flowfields," *Journal of Propulsion and Power*, Vol. 2, No. 1, 1986, pp. 4–10.

[24]Holdeman, J. D., "A Numerical Study of the Effects of Curvature and Convergence on Dilution Jet Mixing," AIAA Paper 87-1953, 1987; also NASA TM 89878.

[25]Holdeman, J. D., "Mixing of Multiple Jets with a Confined Subsonic Crossflow," *Progress in Energy and Combustion Science*, Vol. 109, No. 1, 1993, pp. 31–70.

[26]Holdeman, J. D., Srinivasan, R., Coleman, E. B., Meyers, G. D., and White, C. D., "Effects of Multiple Rows and Non-Circular Orifices on Dilution Jet Mixing," *Journal of Propulsion and Power*, Vol. 3, No. 3, 1987, pp. 219–226.

[27]Zhu, G., Lai, M.-C., and Xiong, T. Y., "Numerical and Experimental Study of the Nonreacting Flowfield in a Cyclonic Combustor," 1992 ASME Cogen Turbo Power, Houston, TX, Sept. 1992.

[28]Smith, C. S., Talpallikar, M. V., and Holdeman, J. D., "A CFD Study of Jet Mixing in Reduced Flow Areas for Lower Combustor Emissions," AIAA Paper 91-2460; also NASA TM 104411, 1991.